Electron-spin resonance in spin-1 planar magnetic chains

N. Papanicolaou
Department of Physics, University of Crete, and Research Center of Crete, Heraklion, Greece

A. Orendáčová and M. Orendáč
Faculty of Science, P. J. Šafárik University, Park Angelinum 9, 04154 Košice, Slovakia

(Received 9 May 1997)

We present a theoretical study of electron-spin resonance (ESR) in spin-1 chains with a strong planar anisotropy and an exchange interaction that is either ferromagnetic or antiferromagnetic. For a sufficiently weak bias field, the ground state carries vanishing azimuthal spin and the resonance spectrum is dominated by transitions to excitons and antiexcitons with azimuthal spin ± 1. When the field exceeds a certain critical value, the ground state is a fully saturated ferromagnet and the relevant elementary excitations are ordinary magnons. The contribution of a two-magnon bound state, often referred to as the single-ion bound state, is of special importance and is analyzed in detail. These theoretical results are consistent with available ESR measurements on $Ni(C_2H_8N_2)_2Ni(CN)_4$ and suggest more detailed experiments. [S0163-1829(97)05438-6]

I. INTRODUCTION

There exist several experimental realizations of spin-1 chains with an easy-plane anisotropy of strength D that is significantly larger than the exchange constant J. For $D>J$, the elementary excitations are separated from the ground state by a nonvanishing energy gap irrespective of whether the exchange interaction is ferromagnetic (FM) or antiferromagnetic (AFM). The gap vanishes at a critical anisotropy $D\sim J$, while a clear distinction between FM and AFM chains emerges in the weak-anisotropy region $D<J$. The former are characterized by gapless modes, as expected, but the latter exhibit an unexpected Haldane gap studied extensively in recent years.[1]

Experimental investigations of spin-1 chains with supercritical anisotropy ($D>J$) have also been carried out by a variety of techniques, such as neutron scattering, specific heat and susceptibility measurements, and electron-spin resonance.[2–5] On the other hand, some theoretical predictions have been obtained by a mean-field approach adapted to strong anisotropy[6] and by a direct strong-coupling expansion.[7]

Our current aim is to provide a calculation of ESR for $D>J$ systems at low temperature that probes directly the elementary excitations. Spin resonance is monitored by a uniform bias field applied along the symmetry (hard) axis and varied over a wide range of values. The weak-field regime is dominated by $\Delta m=\pm 1$ transitions between the ground state and (anti)excitons that are accurately accounted for by the strong-coupling expansion when $D\gg J$. Above a certain critical value of the bias field the ground state is ordered and the main contributions originate in transitions to magnons, as well as transitions between magnons and two-magnon states. A distinct role is played by the single-ion bound state originally calculated by Silberglitt and Torrance[8] for easy-axis ferromagnets and later extended to easy-plane magnetic chains above the spin-flop transition by Papanicolaou and Psaltakis.[9]

The main assertion of the present paper is that spin-1 chains with a strong planar anisotropy provide an appropriate setting for a more or less direct observation of the single-ion bound state. We shall further argue that available ESR data[4,5] from $Ni(C_2H_8N_2)_2Ni(CN)_4$, usually referred to with the abbreviated symbol NENC, are consistent with the above assertion. The problem is formulated in Sec. II and solved for FM and AFM exchange in Secs. III and IV, respectively. The main conclusions are summarized in Sec. V, whereas the Appendix is devoted to a survey of the calculation of the single-ion bound state.

II. FORMULATION

We consider the class of spin-1 magnetic chains governed by the Hamiltonian

$$W=\sum_n \left[D(S_n^z)^2 \pm J(\mathbf{S}_n\cdot\mathbf{S}_{n+1})+g\mu_B(\mathbf{H}\cdot\mathbf{S}_n)\right], \quad (2.1)$$

where both the anisotropy constant D and the exchange constant J are taken to be positive and the distinction between AFM and FM chains is made explicit by the $\pm$ choice in Eq. (2.1). Since our aim is to study mainly the case of strong anisotropy, it is convenient to scale out the anisotropy constant by measuring energy in units of D. The remaining independent parameters are the dimensionless ratios

$$\rho=J/D, \quad \mathbf{h}=g\mu_B\mathbf{H}/D. \quad (2.2)$$

The region of current interest is $\rho\ll 1$ but no restriction is imposed on the strength of the bias field h.

In a typical ESR experiment a microwave field of frequency ω is applied in the basal plane along, say, the x axis. The power absorption is proportional to $\omega\chi''(\omega)$ where the imaginary part of the susceptibility is given by

$$\chi''(\omega)=\frac{1}{2}(1-e^{-\beta\omega})\int_{-\infty}^{\infty} dt e^{i\omega t}\langle\mu_x(t)\mu_x(0)\rangle_T. \quad (2.3)$$

Here $\langle\cdots\rangle_T$ is the usual thermal average and $\mu_x=\Sigma_n S_n^x$ is the total spin in the x direction. To complete the description of rationalized units we note that $\beta=1/T$, where T is the temperature in units of D, and the unit for the frequency ω is $D/\hbar$. Therefore neither the anisotropy nor the Planck constant will appear explicitly in our calculations.

An exact calculation of $\chi''(\omega)$ is out of question except in the limit of vanishing exchange constant ($\rho=0$). This limit provides a valuable guide for understanding magnetic chains with $\rho\ll 1$ and is discussed in some detail in the present section. Thus, at $\rho=0$, spins uncouple and the trace in Eq. (2.3) may be restricted to the eigenstates of the single-spin Hamiltonian $W=(S^z)^2+(\mathbf{h}\cdot\mathbf{S})$ written in rationalized units. Let us consider the case of a bias field applied along the hard axis; $\mathbf{h}=(0,0,h)$. The eigenstates are then given by the canonical spin-1 basis $|1,0\rangle$, $|1,\pm 1\rangle$ with eigenvalues

$$\varepsilon_0=0, \quad \varepsilon_\pm=1\pm h; \quad z=1+e^{-\beta\varepsilon_+}+e^{-\beta\varepsilon_-}, \quad (2.4)$$

where we also quote the expression for the partition function z at a single site. A straightforward application of Eq. (2.3) yields

$$\chi''(\omega)=\frac{N\pi}{2z}[(1-e^{-\beta\varepsilon_+})\delta(\varepsilon_+-\omega)+(1-e^{-\beta\varepsilon_-})\times\delta(\varepsilon_--\omega)+(e^{-\beta\varepsilon_+}-1)\delta(\varepsilon_++\omega)+(e^{-\beta\varepsilon_-}-1)\delta(\varepsilon_-+\omega)], \quad (2.5)$$

where N is the total number of sites and appears as an overall factor. As expected, $\chi''(\omega)$ is an odd function of frequency and only two out of the four terms survive at positive frequencies. However the terms that survive depend on the strength of the bias field because level crossing occurs at the critical value $h=h_c=1$.

For $h<1$, the energy levels are ordered as $\varepsilon_+>\varepsilon_->\varepsilon_0=0$ and only the first two terms in Eq. (2.5) survive when $\omega>0$. The first term corresponds to a $\Delta m=1$ transition between the ground state $|1,0\rangle$ and the ''exciton'' $|1,1\rangle$ while the second to a $\Delta m=-1$ transition between $|1,0\rangle$ and the ''antiexciton'' $|1,-1\rangle$. The resonance frequencies are given by

$$\omega_A=\varepsilon_+-\varepsilon_0=1+h, \quad \omega_B=\varepsilon_--\varepsilon_0=1-h \quad (2.6)$$

and the corresponding intensities may be inferred from the coefficients of the δ functions in Eq. (2.5) multiplied by the frequency ω. One should note that the intensities of the exciton and the antiexciton are different at nonvanishing field; in particular, the intensity of the antiexciton vanishes at the critical field $h=1$ for all temperatures. For $h>1$, the energy levels are ordered as $\varepsilon_+>\varepsilon_0=0>\varepsilon_-$ and the state $|1,-1\rangle$ is now the ground state. At positive frequencies only the first and fourth terms in Eq. (2.5) survive. The fourth term corresponds to a $\Delta m=1$ transition between the ''ferromagnetic'' ground state $|1,-1\rangle$ and the ''magnon'' $|1,0\rangle$ while the first to a transition between the magnon and the ''single-ion bound state'' $|1,1\rangle$. (This terminology will become more meaningful when the exchange interaction is turned on.) The respective resonance frequencies are

$$\omega_C=\varepsilon_0-\varepsilon_-=h-1, \quad \omega_D=\varepsilon_+-\varepsilon_0=h+1. \quad (2.7)$$

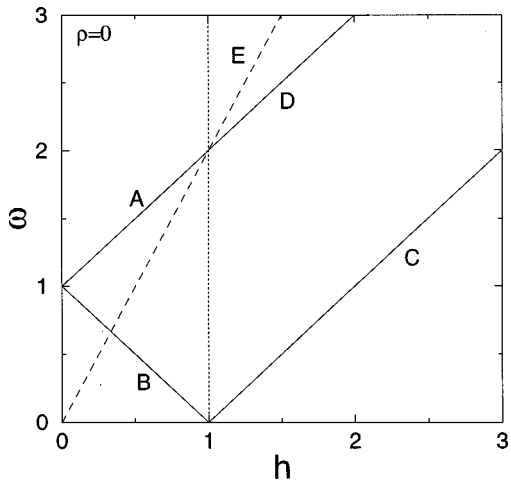

FIG. 1. Field dependence of the resonance lines at vanishing exchange interaction and a bias field pointing along the hard axis. The $\Delta m=2$ resonance E is depicted by a dashed line to indicate that its intensity vanishes within the single-spin model. Here and in all subsequent illustrations the frequency ω is measured in units of $D/\hbar$ and the field h in units of $D/g\mu_B$.

A notable feature of the first term in Eq. (2.5) is that the intensity of the transition $|1,0\rangle\rightarrow|1,1\rangle$ vanishes at zero temperature, because the transition takes place between excited states, except at the critical field $h=1$ where the intensity remains finite even at $T=0$.

The preceding elementary results are schematically summarized in Fig. 1 which plots the resonance frequencies (2.6) and (2.7) as a functions of the bias field for $h<1$ and $h>1$, respectively. In all cases the resonance lines are straight because the bias field preserves the azimuthal symmetry. One should also note that line D for $h>1$ is the continuation of line A for $h<1$. However the temperature dependence of the corresponding intensities is significantly different in the two regions; for example, line D looses its intensity at $T=0$ for all fields except the critical one $h=1$.

The resonance spectrum observed in NENC agrees with Fig. 1 in its gross features, with two important deviations.[4,5] First, the experimentally observed line D is no longer the continuation of line A apparently due to the effect of a small but nonvanishing exchange interaction, which will be analyzed in detail in Secs. III and IV. Second, there is evidence for an additional resonance that corresponds to a (normally) forbidden $\Delta m=2$ transition. Within the single-spin model discussed so far such a transition would yield a frequency

$$\omega_E=\varepsilon_+-\varepsilon_-=2h, \quad (2.8)$$

depicted as line E in Fig. 1, which is in rough agreement with experiment. Of course, the intensity of this resonance vanishes within the single-spin model. A nonvanishing intensity could be achieved through mixing of states of definite azimuthal spin produced by the combined effect of an in-plane anisotropy of the form $E[(S^x)^2-(S^y)^2]$ and the exchange interaction. For simplicity, the potential effects of the E term will not be discussed further in the present paper.

This section is completed with a brief discussion of the case of a bias field applied in the basal plane; e.g., **h**

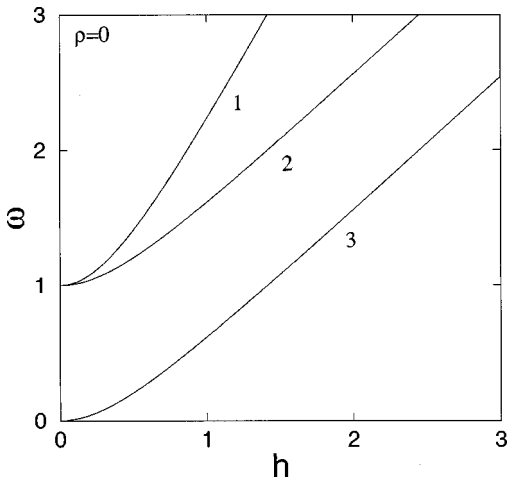

FIG. 2. Field dependence of the resonance lines at vanishing exchange interaction and a bias field applied in the basal plane.

$=(h,0,0)$. At $\rho=0$, the relevant single-spin Hamiltonian is $W=(S^z)^2+hS^x$ and its eigenvalues

$$\varepsilon_0=1, \quad \varepsilon_\pm=\frac{1}{2}\pm\sqrt{\frac{1}{4}+h^2}, \tag{2.9}$$

are ordered as $\varepsilon_-<\varepsilon_0<\varepsilon_+$ for all values of the bias field. The possible resonance frequencies are then given by

$$\omega_1=\varepsilon_+-\varepsilon_-=2\sqrt{\frac{1}{4}+h^2},$$

$$\omega_2=\varepsilon_0-\varepsilon_-=\sqrt{\frac{1}{4}+h^2}+\frac{1}{2},$$

$$\omega_3=\varepsilon_+-\varepsilon_0=\sqrt{\frac{1}{4}+h^2}-\frac{1}{2}, \tag{2.10}$$

and are plotted in Fig. 2 as functions of the applied field. We shall not quote here the complete expression for $\chi''(\omega)$ but mention that the intensities of the various modes depend on the relative orientation of the bias and microwave fields, both lying in the basal plane. Figure 2 already provides a rough approximation of the observed resonances in chains with a small exchange interaction immersed in a transverse bias field.[2–5] In particular, line 3 was termed a ''single-ion'' mode[10] and involves transitions between excited states and thus its intensity vanishes at $T=0$; in this respect, resonance 3 in Fig. 2 is analogous to resonance D in Fig. 1. Actually the latter is a better candidate for a detailed study of the single-ion mode at nonvanishing exchange. Therefore the effects of a transverse bias field will not be considered further in this paper.

III. FERROMAGNETIC EXCHANGE

We now come to the main point, namely the calculation of the effect of a small but nonvanishing exchange interaction. Throughout this section we consider ferromagnetic exchange and a bias field that points along the hard axis. Expressed in rationalized units the relevant Hamiltonian is

$$W=\sum_n\,[(S_n^z)^2-\rho(\mathbf{S}_n\cdot\mathbf{S}_{n+1})+hS_n^z]. \tag{3.1}$$

A direct calculation of the susceptibility from Eq. (2.3) is no longer possible but we will, instead, locate the most important contributions at low temperature using the equivalent expression[11]

$$\chi''(\omega)=\frac{\pi}{Z}\sum_{a,b}\,(e^{-\beta E_b}-e^{-\beta E_a})|\langle a|\mu_x|b\rangle|^2\delta(E_a-E_b-\omega), \tag{3.2}$$

where sums extend over all eigenstates $|a\rangle$ of Hamiltonian (3.1) and E_a are the corresponding eigenvalues. Accordingly Z is the total partition function that should be distinguished from the single-site partition function z of Sec. II.

In order to arrive at a successful strategy for $0<\rho\ll 1$, it is useful to briefly analyze the $\rho=0$ results of Sec. II from the point of view of Eq. (3.2) that entails sums over all eigenstates of the complete chain with N spins. Thus, at $\rho=0$ and $h<1$, the ground state Ω is nondegenerate and such that all sites carry vanishing azimuthal spin ($m=0$) and vanishing energy ($E_0=0$). An exciton (e) or antiexciton ($\overline{e}$) state is obtained by exciting any single site to an azimuthal spin $m=1$ or -1; there exist N independent e states, each with energy $E_e=\varepsilon_+=1+h$, and an equal number of $\overline{e}$ states with energy $E_{\overline{e}}=\varepsilon_-=1-h$. The process may be continued in an obvious way to construct $N(N-1)/2$ two-exciton (ee) states with $m=2$ and $E_{ee}=2\varepsilon_+$, an equal number of two-antiexciton ($\overline{e}\,\overline{e}$) states with $m=-2$ and $E_{\overline{e}\,\overline{e}}=2\varepsilon_-$, $N(N-1)$ exciton-antiexciton ($e\overline{e}$) states with $m=0$ and $E_{e\overline{e}}=\varepsilon_++\varepsilon_-$, and so on. One may then identify the $\Delta m=1$ transitions in Eq. (3.2) as $\Omega\to e$, $e\to ee$, $\overline{e}\to e\overline{e},\ldots$, all of which lead to a common resonance frequency $\omega=\varepsilon_+$, as well as the $\Delta m=-1$ transitions $\Omega\to\overline{e}$, $\overline{e}\to\overline{e}\,\overline{e}$, $e\to e\overline{e},\ldots$, with resonance at $\omega=\varepsilon_-$. A straightforward calculation of the corresponding matrix elements in Eq. (3.2) at $\rho=0$ leads to

$$\chi''(\omega)=\frac{N\pi}{2Z}\,[1+(N-1)(e^{-\beta\varepsilon_+}+e^{-\beta\varepsilon_-})+\cdots]$$
$$\times[(1-e^{-\beta\varepsilon_+})\,\delta(\varepsilon_+-\omega)$$
$$+(1-e^{-\beta\varepsilon_-})\,\delta(\varepsilon_--\omega)]. \tag{3.3}$$

To make contact with Eq. (2.5) we note that $Z=z^N$ and

$$[1+(N-1)(e^{-\beta\varepsilon_+}+e^{-\beta\varepsilon_-})+\cdots]=z^{N-1}, \tag{3.4}$$

when all higher-order processes are included. Equation (3.3) then reduces to Eq. (2.5) applied for $h<1$ and $\omega>0$.

The main feature of the preceding elementary calculation is that all $\Delta m=1$ (or $\Delta m=-1$) transitions lead to a common resonance frequency in Eq. (3.3) and the corresponding contributions to the intensity add up coherently in Eq. (3.4) to produce the correct linear dependence on N anticipated in Eq. (2.5). When the exchange interaction is turned on, the various processes do not lead to a common transition frequency, thus causing the familiar line broadening. However, at low temperature, the basic resonance is still due to the fundamental $\Omega\to e$ transition, while the higher-order processes $e\to ee$, $\overline{e}\to e\overline{e},\ldots$, are responsible for the observed

finite linewidth and possibly a mild temperature-dependent frequency shift of the maximum of the intensity.

Therefore, for $\rho \neq 0$, the main effect at low temperature may be obtained by keeping only the first few terms in Eq. (3.2) and by calculating the necessary energy eigenvalues and matrix elements using the strong-coupling expansion of Ref. 7. Because the bias field preserves the azimuthal symmetry, the energy of an exciton or antiexciton at crystal momentum k is given by

$$\varepsilon_{\pm}(k) = \varepsilon(k) \pm h,$$
$$\varepsilon(k) = 1 - 2\cos k\rho + (1 + 2\sin^2 k)\rho^2 + \left[\frac{1}{2}(1 + 8\sin^2 k)\cos k - 2\sin^2 k\right]\rho^3 + \cdots, \tag{3.5}$$

where $\varepsilon(k)$ is the common (anti)exciton dispersion calculated in Ref. 7 at vanishing field. ESR transitions from the ground state take place only to $k=0$ excitons and antiexcitons and the corresponding resonance frequencies are

$$\omega_A = \varepsilon_+(k=0) = \left(1 - 2\rho + \rho^2 + \frac{1}{2}\rho^3 + \cdots\right) + h,$$
$$\omega_B = \varepsilon_-(k=0) = \left(1 - 2\rho + \rho^2 + \frac{1}{2}\rho^3 + \cdots\right) - h, \tag{3.6}$$

which generalize Eqs. (2.6) to finite ρ. The most important contributions in Eq. (3.2) are then given by the $(k=0)$ transitions $\Omega \to e$ and $\Omega \to \bar{e}$ that lead to

$$\chi''(\omega) \approx \frac{N\pi f_0}{2Z}\left[(1 - e^{-\beta\omega_A})\,\delta(\omega_A - \omega) + (1 - e^{-\beta\omega_B})\,\delta(\omega_B - \omega)\right], \tag{3.7}$$

where the amplitude f_0 may be inferred from Eq. (4) of Ref. 7 applied for $k=0$:

$$f_0 = 1 + 2\rho + \frac{3}{2}\rho^2 + \cdots. \tag{3.8}$$

One should further note the total partition function Z can also be calculated within the strong-coupling expansion.[7] However it is not especially meaningful to use the result of the above reference in Eq. (3.7) because the latter neglects higher-order processes and is strictly valid at $T=0$ where $Z=1$ and

$$T=0; \quad \chi''(\omega) = \frac{1}{2} N\pi f_0[\delta(\omega_A - \omega) + \delta(\omega_B - \omega)]. \tag{3.9}$$

The only approximation remaining in Eq. (3.9) is related to the fact that the frequencies ω_A, ω_B and the amplitude f_0 are given by the truncated series (3.6) and (3.8) that are fairly accurate for $\rho \ll 1$.

The calculated frequencies (3.6) are plotted as lines A and B in Fig. 3, which are still straight lines and differ from those of Fig. 1 only by a downward parallel displacement due to the exchange interaction. To be sure, A and B are the $T \to 0$ limits of the resonances actually observed in an experiment at finite temperature where line broadening occurs thanks to higher-order processes. A related fact is that the maxima of the power absorption may acquire a mild temperature dependence, and a field dependence that deviates from a straight line, because the intensities of higher-order processes do not add up coherently when $\rho \neq 0$. The essence of the above remarks is captured by a self-consistent approximation employed in Ref. 10 for the analysis of ESR data from $CsFeCl_3$. Line broadening of exciton and antiexciton spectra will not be discussed further in the present paper. In particular, we do not consider the effect of exciton bound states[7] whose ESR signal may add some interesting fine structure to the observed broadened resonances but is not expected to be conspicuous.

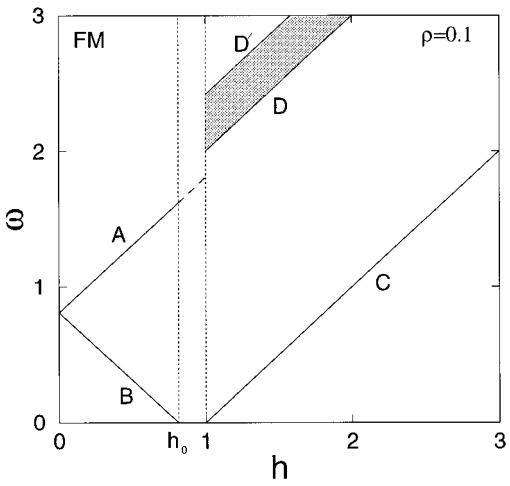

FIG. 3. Field dependence of the ESR spectrum for a ferromagnetic chain with a small exchange interaction ($\rho = 0.1$). The exciton line A is continued as a dashed line into the spin-flop regime ($h_0 < h < h_c = 1$) to indicate our present lack of knowledge of the low-lying excitation spectrum for such field values; see the text for further explanations.

Instead, we return to Fig. 3 and note that the antiexciton branch B terminates on the horizontal axis at a field value $h = h_0$. Since the smallest gap occurs at the zone center the critical field h_0 is determined from the condition $\varepsilon_-(k=0) = 0$ or

$$h_0 = 1 - 2\rho + \rho^2 + \frac{1}{2}\rho^3 + \cdots < 1, \tag{3.10}$$

where level crossing occurs and the ground state ceases to be an (azimuthal) spin singlet. Above h_0 the chain enters a spin-flop phase where the ground state becomes increasingly ferromagnetic. Complete ferromagnetic order is achieved above a critical field h_c that coincides with the value $h_c = 1$ of the single-spin model of Sec. II. The remainder of this section is devoted to the calculation of the ESR spectrum above the spin-flop transition ($h > 1$) where detailed theoretical information is available on the low-lying excited states[9] and is briefly reviewed in the Appendix.

The excitation spectrum is depicted in Fig. 4 for a typical small exchange constant $\rho = 0.1$ and a bias field $h = 3/2 > h_c = 1$. The low-lying spectrum consists of the usual magnon with a dispersion

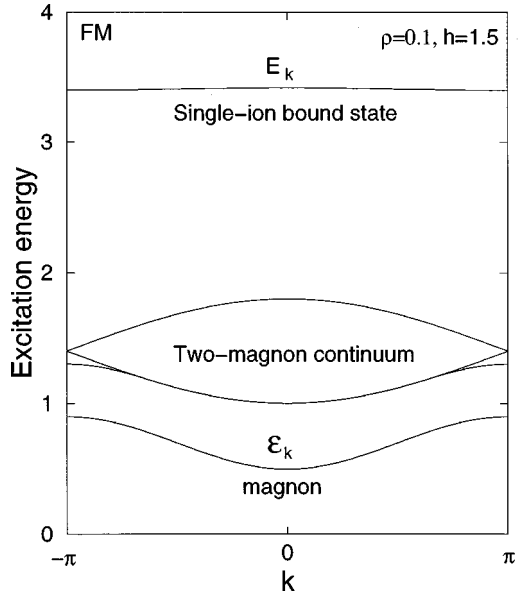

FIG. 4. One- and two-magnon excitation energies (in units of D) for a ferromagnetic chain with a small exchange interaction ($\rho=0.1$) and a typical field above the spin-flop regime ($h=h_c+1/2=1.5$). For this small value of ρ the single-ion bound state is well separated above the continuum while the exchange bound state branches off below the continuum near the zone boundary.

$$\varepsilon_k = h-1+2\rho(1-\cos k) \tag{3.11}$$

that confirms the critical field $h_c=1$; for $h<1$, the magnon energy becomes negative at $k=0$, thus signaling instability of the fully ordered ground state. Furthermore two-magnon states come in three varieties: a two-magnon continuum with boundaries at $2(h-1)+4\rho[1\pm\cos(k/2)]$, an ''exchange'' bound state that branches off below the continuum near the zone boundary, and a ''single-ion''bound state that extends throughout the zone and is well separated above the continuum when $\rho\ll 1$. The single-ion mode is of special importance in the following and its exact energy-momentum dispersion is given by

$$E_k = 2(h-1)+4\rho\left[1+\frac{1}{2}\left(x+\frac{1}{x}\right)\cos\frac{k}{2}\right], \tag{3.12}$$

where x is the appropriate root of the cubic equation (A8) discussed in the Appendix, whose accurate numerical calculation is straightforward. Nevertheless, for all practical purposes in the parameter region of current interest, an excellent approximation is obtained by

$$x\approx\rho\left(1+\frac{\rho^3}{2+\rho}\cos^2\frac{k}{2}\right)\cos\frac{k}{2}. \tag{3.13}$$

In fact, in order to be consistent with our earlier discussion of excitons and antiexcitons, the single-ion dispersion (3.12) may be approximated by inserting Eq. (3.13) and consistently expanding to third order in ρ to obtain

$$E_k\approx 2(h-1)+2\left[1+2\rho+\left(\rho^2-\frac{1}{2}\rho^3\right)\cos^2\frac{k}{2}\right], \tag{3.14}$$

which is actually exact at the zone boundary ($k=\pi$) for all ρ, and fairly accurate at the zone center ($k=0$) for $\rho\ll 1$. This approximate dispersion may be used safely in the range $\rho\lesssim 0.3$ that encompasses most known magnetic chains with supercritical anisotropy. Otherwise one must resort to the exact dispersion (3.12) which is valid for all ρ including $\rho>1$.

For $h>1$, the only ESR transition that survives in the limit $T\to 0$ is the one between the ferromagnetic ground state and a single magnon with $k=0$. It is thus useful to write the susceptibility as

$$\chi''(\omega)=\chi_1''(\omega)+\chi_2''(\omega), \tag{3.15}$$

where χ_1'' is the single-magnon contribution and χ_2'' contains all other ($\Delta m=1$) processes that acquire a nonvanishing intensity at finite temperature. The former is easily calculated by identifying the single-magnon term in the sum of Eq. (3.2) to obtain

$$\chi_1''(\omega)=\frac{N\pi}{2Z}\,(1-e^{-\beta\omega_C})\,\delta(\omega_C-\omega),$$

$$\omega_C=\varepsilon_{k=0}=h-1, \tag{3.16}$$

where ω_C coincides with the corresponding frequency in the limit $\rho=0$, see Eq. (2.7), and is plotted as line C in Fig. 3 for $h>1$. For future reference we also quote the total power absorbed by the single-magnon process:

$$P_1\sim\int\omega\chi_1''(\omega)d\omega=\frac{N\pi\omega_C}{2Z}\,(1-e^{-\beta\omega_C}), \tag{3.17}$$

which vanishes at the critical field $h=1$ for all temperatures, because a magnon with $k=0$ becomes degenerate with the ground state, but increases with h for $h>1$. Finally we recall that Eqs. (3.16) and (3.17) are strictly appropriate at $T=0$ where they yield the *complete* susceptibility $\chi''(\omega)$ and power absorption P:

$$T=0;\quad \chi''(\omega)=\frac{1}{2}\,N\pi\delta(\omega_C-\omega),\quad P\sim\frac{1}{2}\,N\pi\omega_C. \tag{3.18}$$

Thus we turn our attention to $\Delta m=1$ processes that occur at finite temperature. The simplest possibility is a transition between a single-magnon and a two-magnon state. Inspection of Fig. 4 suggests that a transition between a magnon and a state in the two-magnon continuum yields a signal that is roughly superimposed with the basic magnon line C and contributes to its broadening, in analogy with the line broadening of excitons and antiexcitons discussed earlier in the text. Similarly a transition between a magnon and an exchange bound state yields a signal in the same frequency range; hence the exchange bound state is not expected to be conspicuous in the observed resonance spectrum. On the contrary, it is evident from Fig. 4 that a transition between a magnon and a single-ion bound state makes a distinct contribution to $\chi_2''(\omega)$ that is clearly separated from the magnon resonance C. In fact, such a process is responsible for the ρ-dependent deformations of line D of Fig. 1 and will be calculated in detail.

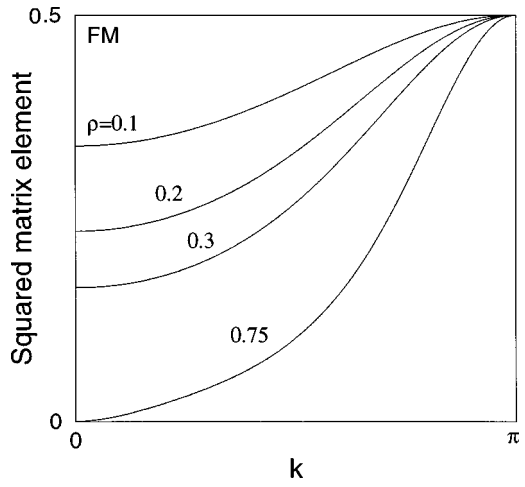

FIG. 5. The squared matrix element (3.22) as a function of crystal momentum for a ferromagnetic chain with various values of $\rho = J/D$.

Specifically, the contribution of the above process may be isolated in Eq. (3.2) to write

$$\chi_2''(\omega) \approx \frac{N}{Z}(1-e^{-\beta\omega})\int_0^\pi dk e^{-\beta\varepsilon_k}|f(k)|^2\delta(\Delta_k-\omega), \tag{3.19}$$

where Z is the total partition function, ε_k is the magnon dispersion (3.11), $\Delta_k = E_k - \varepsilon_k$ is the energy difference between the single-ion mode and the magnon at crystal momentum k (see Fig. 4), and $f(k) = \langle \psi_2(k)|\mu_x|\psi_1(k)\rangle$ is the matrix element of the total moment between the corresponding normalized wave functions. The exact expression for Δ_k is readily computed from Eqs. (3.11) and (3.12):

$$\Delta_k = h - 1 + \frac{2\rho}{x}\left(1 + 2x\cos\frac{k}{2} + x^2\right)\cos\frac{k}{2}, \tag{3.20}$$

and may be approximated to third order by

$$\Delta_k \approx h + 1 + (4\rho + 2\rho^2 - \rho^3)\cos^2\frac{k}{2}. \tag{3.21}$$

Also using the explicit wave functions constructed in the Appendix we have calculated the (exact) matrix element

$$|f(k)|^2 \equiv \frac{X}{2Y},$$

$$X = \left[1 - \frac{2[x+\cos(k/2)]}{1+2x\cos(k/2)+x^2}\left(x + \frac{1}{x} - \frac{1}{\rho\cos(k/2)}\right)\right]^2,$$

$$Y = 1 + \frac{1}{1-x^2}\left(x + \frac{1}{x} - \frac{1}{\rho\cos(k/2)}\right)^2, \tag{3.22}$$

which may be approximated at small ρ through Eq. (3.13). Incidentally, in all of the ensuing graphical illustrations we have used a precise numerical calculation of the root x of the cubic equation.

For example, the result of Eq. (3.22) is plotted in Fig. 5 as a function of crystal momentum for various values of ρ. The squared matrix element approaches the free-spin value 1/2 at the zone boundary for all ρ, and the same value for all k when $\rho \to 0$. On the other hand, significant departures from the free-spin model occur at the zone center with increasing ρ. At $\rho = 3/4$ the matrix element vanishes for $k = 0$, so does the energy gap between the single-ion bound state and the upper side of the two-magnon continuum. The fate of the bound-state spectrum for $\rho > 3/4$ is further discussed in the Appendix but is irrelevant for the parameter region of current interest where the single-ion bound state is well separated from the continuum and both its dispersion E_k and the matrix element $|f(k)|^2$ are nearly flat through the zone. Nonetheless sufficient structure persists at small ρ that should lead to a clear ESR signal for the single-ion bound state.

Indeed, we now return to Eq. (3.19) and note that absorption occurs for frequencies that satisfy the resonance condition

$$\omega = \Delta_k, \tag{3.23}$$

i.e., for frequencies in the band $\omega_D < \omega < \omega_{D'}$, where ω_D and $\omega_{D'}$ can be calculated from Eqs. (3.23) and (3.20) applied for $k = \pi$ and $k = 0$:

$$\omega_D = h + 1, \quad \omega_{D'} = h - 1 + \frac{2\rho}{x}(1+x)^2. \tag{3.24}$$

The first relation was obtained by using the fact that the root x vanishes at the zone boundary $k \sim \pi$, as $x \sim \rho\cos(k/2)$, whereas the second relation contains the root x calculated at the zone center. A good approximation of the latter is given by Eq. (3.13), applied for $k = 0$, and a corresponding third-order approximation of the edge frequencies (3.24) reads

$$\omega_D = h + 1, \quad \omega_{D'} = h + 1 + 4\rho + 2\rho^2 - \rho^3 + \cdots, \tag{3.25}$$

which are plotted in Fig. 3 as lines D and D', respectively. The line D coincides with its $\rho = 0$ counterpart in Fig. 1 but is no longer the continuation of the exciton line A that acquires a nontrivial ρ dependence given by Eq. (3.6). Therefore absorption by the single-ion bound state is distributed over a frequency band with a width

$$\Delta = \omega_{D'} - \omega_D = 4\rho + 2\rho^2 - \rho^3 + \cdots \tag{3.26}$$

that remains finite even at very low temperatures and vanishes only when $\rho = 0$. In other words, the single-ion bandwidth Δ must not be confused with ordinary line broadening of elementary excitations.

Our last task is to determine the detailed distribution of power absorption over the DD' band of Fig. 3. Performing the k integration in Eq. (3.19) yields

$$\chi_2''(\omega) \approx \frac{N}{Z}(1-e^{-\beta\omega})e^{-\beta\varepsilon_k}d(k), \tag{3.27}$$

where

$$d(k) = \frac{|f(k)|^2}{|\Delta_k'|} \tag{3.28}$$

is the ''density of states'' and Δ_k' is the k derivative of Δ_k. It is understood that the crystal momentum is expressed as a function of frequency through the resonance condition (3.23)

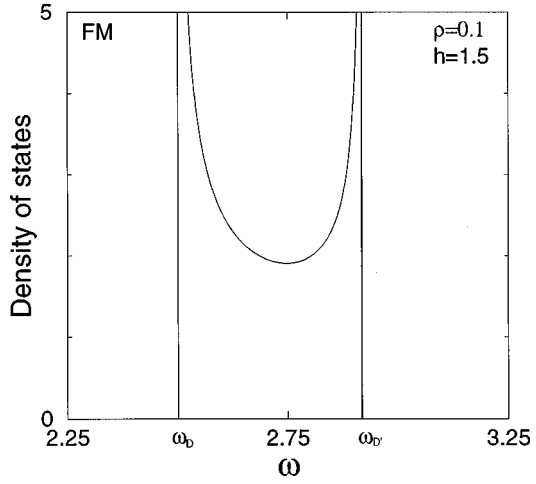

FIG. 6. The density of states (3.25) as a function of frequency for a ferromagnetic chain with $\rho=0.1$. The specific value of the applied field ($h=h_c+1/2=1.5$) does not affect the shape of the density but merely sets the relative position of the DD' band along the frequency axis.

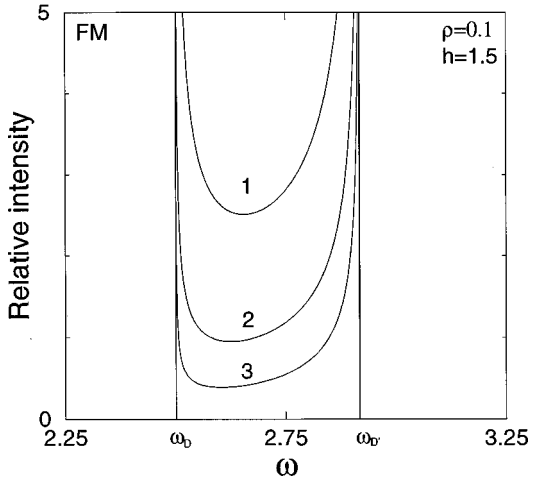

FIG. 7. The relative intensity (3.30) as a function of frequency for a ferromagnetic chain with $\rho=0.1$ and a typical field above the spin-flop regime ($h=1.5$). The intensity of the single-ion mode decreases with decreasing temperature ($T_1=1/2$, $T_2=1/3$, and $T_3=1/4$, in units of D) and eventually vanishes at $T=0$.

viewed as an algebraic equation for $k=k(\omega)$. Actually we need not solve this equation explicitly because the necessary graphs can be produced by calculating Eqs. (3.27) and (3.28) over a dense set of points in $0\leqslant k\leqslant\pi$ and by determining the corresponding frequencies from Eq. (3.23).

The density of states (3.28) is plotted as a function of frequency in Fig. 6 and exhibits the characteristic square-root singularities at the two edges of the DD' band. To make this fact completely explicit we may use the analytical approximation for Δ_k given by Eq. (3.21) to calculate Δ_k' and subsequently enforce the resonance condition (3.23) to obtain

$$|\Delta_k'|\approx[(\omega_{D'}-\omega)(\omega-\omega_D)]^{1/2}. \tag{3.29}$$

Therefore, although nonvanishing absorption occurs throughout the DD' band, a significant enhancement should be expected around the band edges.

Now the intensity of the single-ion process vanishes at $T=0$, except for $h=1$, and an absolute statement cannot be made at finite temperature because we have neglected higher-order processes that are, nonetheless, reflected in the total partition function Z present in Eq. (3.27). Yet the essential point of this calculation can be made by considering the relative intensity,

$$R=\frac{\omega\chi_2''(\omega)}{P_1}=\frac{2}{\pi}\frac{\omega}{\omega_C}\frac{1-e^{-\beta\omega}}{1-e^{-\beta\omega_C}}e^{-\beta\varepsilon_k}d(k), \tag{3.30}$$

with respect to the total absorption P_1 of the single-magnon process given by Eq. (3.17). The relative intensity is then plotted as a function of frequency, in Fig. 7, for three characteristic values of $\beta=1/T$ in the low-temperature region ($T<1\equiv D$). The net conclusion is that absorption should indeed be observed throughout the band, but with a visible enhancement around the band edges.

The effect of the neglected higher-order $\Delta m=1$ processes is twofold. First, multimagnon states with a dominant ''exchange'' component should contribute to normal line broadening of the basic magnon resonance C, with a possibly interesting fine structure due to the exchange bound state. Second, multimagnon states with a significant ''single-ion'' component should cause further broadening of the DD' band, beyond its $T=0$ width Δ of Eq. (3.26), and possibly normalize the square-root singularities of Fig. 7 to two rounded peaks that might merge into one at high temperatures. We have also not carried out a study of the spin-flop phase ($h_0<h<h_c$) and thus cannot ascertain how the exciton spectrum, for $h<h_0$, will join smoothly with the magnon spectrum, for $h>1$.

Nevertheless our theoretical calculation is sufficiently detailed to guide current experiments. In order to achieve a favorable experimental situation, one needs a ferromagnetic compound with a small $\rho=J/D$, so that the DD' band is clearly separated from the (broadened) magnon resonance C, and a critical field $h_c=1$ or $H_c=D/g\mu_B$ that is accessible. $CsFeCl_3$ is a candidate with a measured[12] critical field $H_c=11.5$ T that is not terribly large. However ESR experiments[2,3] have so far been carried out in the region $H<H_c$ and generally confirm the exciton and antiexciton lines A and B of Fig. 3 but yield no information on the spectrum calculated in the present paper for $H>H_c$. Furthermore a considerable uncertainty exists concerning the precise values of the parameters. The parameters extracted from the mean-field approximation of Lindgard[6] differ from those obtained within the strong-coupling expansion[7] as well as those in the self-consistent approach of Suzuki and Makino.[10] A more favorable situation seems to be provided at present by the antiferromagnetic compound NENC studied in the following section.

IV. ANTIFERROMAGNETIC EXCHANGE

Our next aim is to adapt the calculation of Sec. III to the case of spin-1 planar magnetic chains with antiferromagnetic exchange, i.e.,

$$W=\sum_n\left[(S_n^z)^2+\rho(\mathbf{S}_n\cdot\mathbf{S}_{n+1})+hS_n^z\right], \tag{4.1}$$

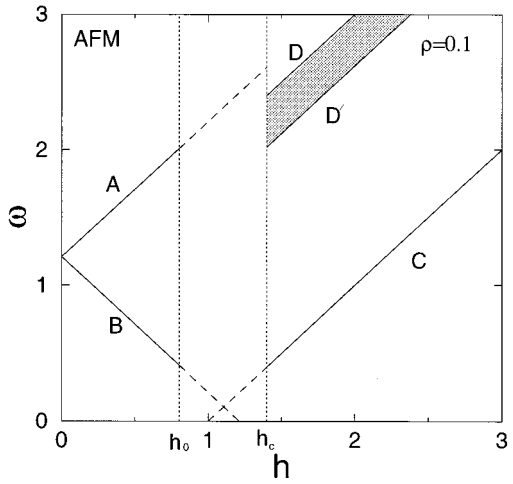

FIG. 8. Field dependence of the ESR spectrum for an antiferromagnetic chain with a small exchange interaction ($\rho=0.1$). The resonance lines A, B, and C are continued as dashed lines into the spin-flop regime ($h_0<h<h_c$) to indicate our present lack of knowledge of the low-lying excitation spectrum for such field values; see the text for further explanations.

where $\rho=J/D$ is again positive. For small ρ and h the ground state is still an azimuthal-spin singlet ($m=0$) and the elementary excitations are $m=1$ excitons and $m=-1$ antiexcitons with dispersions

$$\varepsilon_{\pm}(k)=\varepsilon(k)\pm h,$$

$$\varepsilon(k)=1+2\cos k\rho+(1+2\sin^2 k)\rho^2 - \left[\frac{1}{2}(1+8\sin^2 k)\cos k-2\sin^2 k\right]\rho^3+\cdots \quad (4.2)$$

that differ from those of Eq. (3.5) by the simple replacement $\rho\rightarrow-\rho$. Therefore the elementary excitations are again separated from the ground state by a finite energy gap, except that the gap is now smallest at the zone boundary ($k=\pi$) rather than the zone center ($k=0$). Nevertheless ESR transitions occur at $k=0$ and the corresponding frequencies are

$$\omega_A=\varepsilon_+(k=0)=\left(1+2\rho+\rho^2-\frac{1}{2}\rho^3+\cdots\right)+h,$$

$$\omega_B=\varepsilon_-(k=0)=\left(1+2\rho+\rho^2-\frac{1}{2}\rho^3+\cdots\right)-h, \quad (4.3)$$

which are plotted as lines A and B in Fig. 8. These lines differ from both their $\rho=0$ and FM counterparts in Figs. 1 and 3 by an upward parallel displacement that depends on ρ. Otherwise the discussion of FM excitons and antiexcitons of Sec. III applies here with minor modifications. For example, the low-temperature intensities may be inferred from Eq. (3.7) or (3.9) applied with frequencies ω_A and ω_B given by Eq. (4.3) and an amplitude

$$f_0=1-2\rho+\frac{3}{2}\rho^2+\cdots . \quad (4.4)$$

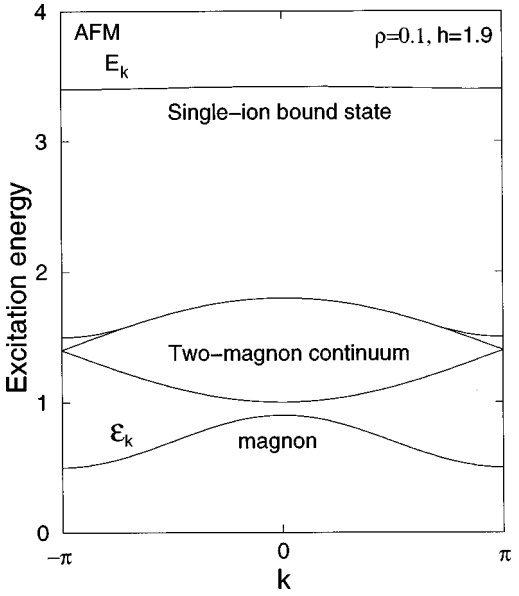

FIG. 9. One- and two-magnon excitation energies (in units of D) for an antiferromagnetic chain with a small exchange interaction ($\rho=0.1$) and a typical field above the spin-flop regime ($h=h_c+1/2=1.9$). For this small value of ρ the single-ion bound state is well separated above the continuum while the exchange bound state branches off also above the continuum near the zone boundary.

The picture becomes slightly more involved with increasing bias field h. Thus the ground state ceases to be a singlet above a critical field h_0 determined from the condition $\varepsilon_-(k=\pi)=0$, because the smallest gap occurs at the zone boundary, or

$$h_0=1-2\rho+\rho^2+\frac{1}{2}\rho^3+\cdots , \quad (4.5)$$

which is identical to the corresponding FM value of Eq. (3.10), at least to third order in ρ. As a consequence, an AFM chain will enter the spin-flop phase well before the antiexciton line B of Fig. 8 touches the field axis. Furthermore the ground state of an AFM chain orders ferromagnetically above a critical field h_c that does not coincide with the $\rho=0$ value $h_c=1$. To locate h_c we note that a completely ordered state is always an eigenstate of the AFM Hamiltonian (4.1) and the dispersion of the single-magnon excitation reads

$$\varepsilon_k=h-h_c+2\rho(1+\cos k), \quad h_c\equiv 1+4\rho. \quad (4.6)$$

The smallest magnon gap occurs at the zone boundary and is equal to $h-h_c$. Therefore, $h_c=1+4\rho$ is the upper critical field and now depends on ρ.

The magnon dispersion (4.6) is depicted in Fig. 9 together with the two-magnon spectrum of an AFM chain calculated in the Appendix. The spectrum consists of a two-magnon continuum with boundaries at $2(h-h_c)+4\rho[1\pm\cos(k/2)]$, an exchange bound state that branches off *above* the continuum near the zone boundary, and a single-ion bound state that is well separated also above the continuum and displays a shape similar to the corresponding FM dispersion of Fig. 4. More precisely, the energy-momentum dispersion of the AFM single-ion bound state is given by

$$E_k = 2(h-h_c) + 4\rho\left[1 + \frac{1}{2}\left(x + \frac{1}{x}\right)\cos\frac{k}{2}\right], \qquad (4.7)$$

where x is the appropriate root of the cubic equation (A19) discussed in the Appendix. For $\rho \ll 1$, an excellent approximation is provided by

$$x \approx \rho\left(1 - \frac{\rho^3}{2-\rho}\cos^2\frac{k}{2}\right)\cos\frac{k}{2} \qquad (4.8)$$

and the exact dispersion (4.7) may be approximated to third order by

$$E_k \approx 2(h-h_c) + 2\left[1 + 2\rho + \left(\rho^2 + \frac{1}{2}\rho^3\right)\cos^2\frac{k}{2}\right]. \qquad (4.9)$$

Accordingly an exact expression for the energy difference $\Delta_k = E_k - \varepsilon_k$ is given by

$$\Delta_k = h - 1 + \frac{2\rho}{x}\left(1 - 2x\cos\frac{k}{2} + x^2\right)\cos\frac{k}{2} \qquad (4.10)$$

and a third-order approximation by

$$\Delta_k \approx h + 1 + (-4\rho + 2\rho^2 + \rho^3)\cos^2\frac{k}{2}, \qquad (4.11)$$

which is actually exact at the zone boundary for all ρ and fairly accurate at the zone center when $\rho \ll 1$.

From this point on the analysis is similar to that of Sec. III and will not be repeated in detail. Thus, for $h > h_c$, the only transition that persists at $T=0$ is the one between the ordered ground state and a $k=0$ magnon, with resonance at frequency

$$\omega_C = \varepsilon_{k=0} = h - h_c + 4\rho = h - 1, \qquad (4.12)$$

which is ρ independent and is again plotted as line C in Fig. 8. The single-magnon intensity is still given by Eq. (3.17) and remains finite at $T=0$, as shown in Eq. (3.18).

Leaving aside broadening effects of the magnon resonance C, including the effect of the exchange bound state, we consider next the deformation of the single-ion resonance D due to the exchange interaction. The contribution of the single-ion bound state is again given by Eq. (3.19) applied with an energy difference Δ_k from Eq. (4.10) and a matrix element

$$|f(k)|^2 \equiv \frac{X}{2Y},$$

$$X = \left[1 - \frac{2[x - \cos(k/2)]}{1 - 2x\cos(k/2) + x^2}\left(x + \frac{1}{x} - \frac{1}{\rho\cos(k/2)}\right)\right]^2, \qquad (4.13)$$

$$Y = 1 + \frac{1}{1-x^2}\left(x + \frac{1}{x} - \frac{1}{\rho\cos(k/2)}\right)^2$$

that differs in its details from the corresponding FM result of Eq. (3.22) and by the fact that x now satisfies a different cubic equation.

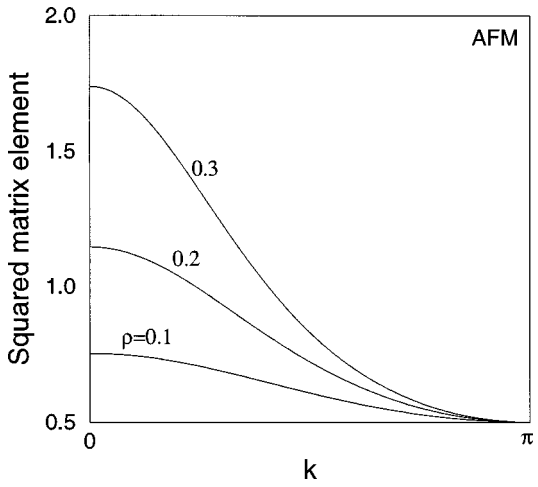

FIG. 10. The squared matrix element (4.13) as a function of crystal momentum for an antiferromagnetic chain with various values of $\rho = J/D$.

A simple inspection of Fig. 9 suggests that absorption takes place over a finite frequency range $\omega_{D'} < \omega < \omega_D$ where the edge frequencies are the values of Δ_k at $k=0$ and $k=\pi$, respectively, or

$$\omega_{D'} = h - 1 + \frac{2\rho}{x}(1-x)^2, \quad \omega_D = h + 1, \qquad (4.14)$$

where x is the root at $k=0$. A third-order approximation is given by

$$\omega_{D'} = h + 1 - 4\rho + 2\rho^2 + \rho^3 + \cdots, \quad \omega_D = h + 1, \qquad (4.15)$$

and the calculated width of the $D'D$ band,

$$\Delta = \omega_D - \omega_{D'} = 4\rho - 2\rho^2 - \rho^3 + \cdots, \qquad (4.16)$$

remains finite even at $T=0$. However nonvanishing absorption is possible only at finite temperature.

The temperature dependence of the intensity is governed by Eq. (3.27) where ε_k is the magnon dispersion (4.6) and the density of states $d(k)$ is calculated from Eq. (3.28) applied with an energy difference Δ_k from Eq. (4.10) or (4.11) and a matrix element $|f(k)|^2$ from Eq. (4.13). The latter is plotted in Fig. 10 in order to point out an important difference from the FM result of Fig. 5; the squared matrix element is greater than the free-spin value 1/2, except at the zone boundary, and increases without bound, at the zone center, with increasing ρ. Such a behavior is intimately related to the fate of the bound-state spectrum for large ρ, or weak anisotropy, and is further discussed in the Appendix. For the region of current interest it is sufficient to note that $|f(k)|^2$ exhibits a mild k dependence throughout the zone. Therefore the structure of the density of states (3.28) is mainly determined by $|\Delta_k'|$ for which a good approximation is obtained from Eqs. (4.11) and (4.15):

$$|\Delta_k'| \approx [(\omega - \omega_{D'})(\omega_D - \omega)]^{1/2}. \qquad (4.17)$$

As a consequence, the density of states is similar to the FM density of Fig. 6, except that the frequency $\omega_{D'}$ now preceeds ω_D. Accordingly the temperature dependence of the

intensity is also similar to the one displayed in Fig. 7 and the qualitative picture discussed in Sec. III applies here almost unchanged. In particular, the intensity of the single-ion resonance diminishes with decreasing temperature but should exhibit an increasingly sharp double-peak structure around the edges of the $D'D$ band. In the extreme low-temperature limit the intensity vanishes but the bandwidth Δ remains finite and is given by Eq. (4.16).

We now examine whether or not the derived picture is consistent with existing ESR data from NENC.[4,5] This is a spin-1 chain with antiferromagnetic exchange, an anisotropy constant $D \approx 6$ K, and a ratio $\rho = J/D \approx 0.13$ that lies well within the domain of validity of the present theoretical calculation. Furthermore the measured critical field, $H_c \approx 4.4$ T, is not too large and thus experiments were performed for both $H < H_c$ and $H > H_c$.

One of the main features of the available data is that the observed single-ion resonance for $H > H_c$ does indeed fall below the continuation of the exciton line A observed for $H < H_c$, in qualitative agreement with Fig. 8. Moreover the observed intensity decreases with decreasing temperature, also in qualitative agreement with the current interpretation.[13] However a quantitative comparison would require more detailed experiments that should clarify the following issues: (a) provide an accurate fit of the exciton and antiexciton resonances A and B of Fig. 8 in the limit $T \to 0$, (b) yield more detailed information on the lower and upper critical fields h_0 and h_c and their relation to the stated experimental value $H_c \approx 4.4$ T in Refs. 4 and 5, (c) obtain further data on the magnon resonance C and possibly examine the manner in which it interpolates into the spin-flop regime, and (d) resolve the predicted double-peak structure of the single-ion band $D'D$ and study the temperature dependence of the corresponding intensity.

V. CONCLUDING REMARKS

We have described but the bare-bones structure of the ESR spectrum at low temperatures for spin-1 planar magnetic chains with either ferromagnetic or antiferromagnetic exchange interaction. Although the derived theoretical results are sufficiently detailed to guide current experiments, the program should be completed with some further theoretical work aimed at the following issues: (a) a study of line-broadening effects, including the potentially interesting fine structure induced by two-exciton as well as two-magnon *exchange* bound states, (b) a calculation in the spin-flop regime ($h_0 < h < h_c$) that would bridge the results for the two regions ($h < h_0$ and $h > h_c$) obtained in this paper, and (c) inclusion of the effects of a weak in-plane anisotropy that is present in realistic compounds and activates normally forbidden ($\Delta m = 2$) transitions, such as the resonance E depicted in Fig. 1 and actually observed in NENC.[4,5]

It would also be of interest to determine the high-temperature limit of the ESR spectrum, for such a limit might be accessible to a detailed theoretical analysis using the method of frequency moments of the imaginary part of the susceptibility.[11] A good starting point is the single-spin result of Eq. (2.5) whose high-temperature limit reads

$$\chi''(\omega) \approx \frac{1}{6} N \pi \beta \omega [\delta(\varepsilon_+ - \omega) + \delta(\varepsilon_- - \omega) + \delta(\varepsilon_+ + \omega) + \delta(\varepsilon_- + \omega)]. \tag{5.1}$$

Therefore the field dependence of the resonance lines is the same as in Fig. 1 and the main simplification at high temperatures concerns the intensities of the various modes. It would thus be useful to study the deformations of Eq. (5.1) effected by the exchange interaction, by calculating a number of moments at finite ρ and then reconstructing the susceptibility by standard methods.[14] However, although a respectable number of moments is available for spin-1/2 chains, we are not aware of a corresponding calculation for spin-1 chains.

Perhaps the most important element of our analysis is the suggestion that the single-ion bound state makes a distinct contribution to the ESR spectrum for $H > H_c$ and its effect can be unambiguously identified. It would be interesting to carry out a similar analysis for easy-axis ferromagnetic chains, originally studied by Silberglitt and Torrance,[8] where the single-ion bound state lies below the two-magnon continuum. Another related problem is that of a spin-1 chain with an additional biquadratic exchange interaction, studied by Chiu-Tsao, Levy, and Paulson,[15] where the single-ion bound state occurs within the continuum and is thus an unstable, yet conspicuous, resonance. A bound-state resonance within the continuum was also found by Hodgson and Parkinson[16] for spin-1 chains with Ising anisotropy.

Finally, there is a potential connection of the single-ion mode with the intrinsic localized spin modes found classically by Wallis, Mills, and Boardman[17] for ferromagnetic chains with an easy-plane single-ion anisotropy, and by Lai, Kiselev, and Sievers[18] for antiferromagnetic chains with an easy-axis single-ion anisotropy. It would certainly be interesting to illuminate such a connection, even though it is difficult to imagine how classical arguments would match in detail the quantum calculation presented in this paper.

ACKNOWLEDGMENT

This work was supported in part by a bilateral Greek-Slovak research program (1996-97).

APPENDIX: TWO-MAGNON STATES

There exist several methods for calculating the two-magnon spectrum in spin-1 chains, the most direct one being based on an elementary Bethe ansatz.[9,16] For chains with ferromagnetic exchange interaction we merely adapt the work of Ref. 9 to current notation and then calculate matrix elements that are necessary for the study of the ESR spectrum in Sec. III. We further extend the calculation to chains with antiferromagnetic exchange interaction and thus provide the basis for the discussion of Sec. IV.

For $h > 1$, the ground state of the FM Hamiltonian (3.1) is given by $|\Omega\rangle = |1,-1\rangle \otimes |1,-1\rangle \otimes \cdots \otimes |1,-1\rangle$, i.e., all spins point along the negative z axis, and its energy is $E_0 = N(1 - \rho - h)$. The single-magnon normalized eigenstate is

$$|\psi_1\rangle = \frac{1}{\sqrt{N}} \sum_{n=1}^{N} e^{ikn}|n\rangle, \tag{A1}$$

where k is the crystal momentum and the state $|n\rangle$ differs from the ground state $|\Omega\rangle$ by the fact that the azimuthal spin at site n is equal to 0 instead of -1. The eigenvalue of $|\psi_1\rangle$ is $E_0+\varepsilon_k$ where ε_k is the magnon excitation energy already quoted in Eq. (3.11). Similarly two-magnon eigenstates are searched for in the form

$$|\psi_2\rangle = \sum_{n=1}^{N-1} \sum_{m=n+1}^{N} c_{n,m}|n,m\rangle + \sum_{n=1}^{N} d_n|n,n\rangle, \tag{A2}$$

where $|n,m\rangle$, with $n \neq m$, differs from the ground state at sites n and m where the azimuthal spin is equal to zero, while $|n,n\rangle$ differs only at site n where the azimuthal spin is equal to $+1$. The coefficients $c_{n,m}$ are given by the familiar Bethe ansatz

$$c_{n,m} = e^{i(k_1 n + k_2 m + \phi/2)} + e^{i(k_1 m + k_2 n - \phi/2)}, \tag{A3}$$

whereas the single-site coefficient is

$$d_n = \frac{\cos(k_1 - \phi/2) + \cos(k_2 + \phi/2)}{\cos k_1 + \cos k_2 + 1/\rho}\, e^{i(k_1+k_2)n} \tag{A4}$$

and differs from the one obtained by extending Eq. (A3) to $n=m$. To complete the ansatz we note that the phase ϕ must satisfy the constraint

$$\cot\frac{\phi}{2} = \frac{(1+Q)\sin[(k_1-k_2)/2]}{2\cos[(k_1+k_2)/2] - (1+Q)\sin[(k_1-k_2)/2]},$$

$$Q \equiv \frac{1+\cos(k_1+k_2)}{\cos k_1 + \cos k_2 + 1/\rho}, \tag{A5}$$

and periodic boundary conditions are enforced if

$$Nk_1 - \phi = 2\pi\lambda_1, \quad Nk_2 + \phi = 2\pi\lambda_2, \tag{A6}$$

where λ_1 and λ_2 are integers that may be restricted to the range $0 \leqslant \lambda_1 \leqslant \lambda_2 \leqslant N-1$. Finally the eigenvalue of $|\psi_2\rangle$ is equal to E_0+E where E_0 is the ground-state energy and

$$E = 2(h-1) + 4\rho\left[1 - \frac{1}{2}(\cos k_1 + \cos k_2)\right] \tag{A7}$$

is the two-magnon excitation energy. The preceding results summarize all necessary information for a complete analysis of the two-magnon spectrum by standard methods.[19]

An immediate consequence of Eq. (A7) is that the boundaries of the two-magnon continuum are located at $2(h-1) + 4\rho[1 \pm \cos(k/2)]$ where $k = k_1 + k_2 \pmod{2\pi}$ is the total crystal momentum restricted to the fundamental Brillouin zone (see Fig. 4). In the following we shall focus on two-magnon *bound states* characterized by complex wave numbers $k_1 = u + iv$ and $k_2 = u - iv$ that may occur when $\lambda_2 = \lambda_1$ or $\lambda_2 = \lambda_1 + 1$, in Eq. (A6), which lead to $\phi = iNv$ or $\pi + iNv$, respectively. In both cases the algebraic constraint (A5) reduces to the cubic equation

$$\rho x^3 + \frac{x^2}{\cos u} + (\rho - 2)x - 2\rho\cos u = 0, \tag{A8}$$

in the thermodynamic limit ($N \to \infty$), where $x = e^{-v}$ may be restricted to the range $0 < x < 1$ without loss of generality. Accordingly the excitation energy (A7) reads

$$E = 2(h-1) + 4\rho\left[1 - \frac{1}{2}\left(x + \frac{1}{x}\right)\cos u\right]. \tag{A9}$$

Therefore, for any given value of $u = (k_1+k_2)/2$ for which Eq. (A8) has a root x in the interval [0,1], Eq. (A9) yields the excitation energy of the corresponding bound state parametrized by the total crystal momentum $k_1 + k_2 = k$ folded into the fundamental Brillouin zone.

The nature of the bound-state spectrum is revealed by first considering Eq. (A8) near the zone boundary ($\cos u \sim 0$) where two real roots emerge

$$x \approx -\rho\cos u \quad \text{or} \quad 2\cos u \tag{A10}$$

that lie in the interval [0,1] provided that $\cos u < 0$ in the first case and $\cos u > 0$ in the second. These roots correspond to the limiting cases of the single-ion and exchange bound states[9] and are examined in turn. The first equation in Eq. (A10) suggests the change of variables

$$x = -\rho\cos u\, z; \quad z = 1 + \frac{z^3\rho^3\cos^2 u}{2+\rho z}, \tag{A11}$$

and the condition $\cos u < 0$ is equivalent to stating that $k = k_1 + k_2$ must take values outside the fundamental zone. We thus effect the usual folding of the zone by the simple prescription $u = k/2 \to k/2 - \pi$ in Eq. (A11) to obtain

$$x = \rho\cos\frac{k}{2}\, z; \quad z = 1 + \frac{z^3\rho^3\cos^2(k/2)}{2+\rho z}, \tag{A12}$$

while the excitation energy (A9) is rewritten in the form given earlier in Eq. (3.12). Now, for each k in the range $[-\pi, \pi]$, the cubic equation in Eq. (A12) is solved by a simple iteration process starting with $z=1$. Actually a single iteration yields a sufficiently accurate description of the single-ion bound state, for $\rho \ll 1$, and the result was already quoted in Eq. (3.13). Similarly the exchange bound state is obtained by starting with the second equation in Eq. (A10) which suggests the change of variables

$$x = 2\cos u\, w; \quad w = 1 - \frac{4\rho w^3\cos^2 u}{\rho + 2w}. \tag{A13}$$

No folding of the zone is required in this case, so we may simply set $u = k/2$ in Eqs. (A9) and (A13) and again solve the cubic equation by simple iteration starting with $w=1$. It is understood that a root x in [0,1] may not be possible for all values of k in the fundamental zone, for either the single-ion or the exchange bound state. The calculated spectrum was illustrated in Fig. 4, for a typical choice of parameters of current interest, and was discussed in Sec. III. Here we complete the description by noting that the single-ion bound state ceases to exist throughout the zone, when $\rho > 3/4$, and branches off above the continuum at some minimum $k = k(\rho)$; see Fig. 2 of Ref. 9. In the extreme limit of vanishing anisotropy ($\rho \to \infty$) the single-ion bound state disappears from the spectrum, while the exchange bound state extends throughout the zone, just below the continuum.

We now consider the calculation of matrix elements that are necessary for the discussion of ESR in Sec. III. First we restrict the general two-magnon wave function (A3) and (A4) to bound states by setting $k_1=u+iv$, $k_2=u-iv$ and $\phi=iNv$; the case $\phi=\pi+iNv$ leads to identical results in the thermodynamic limit and will not be considered explicitly. Hence

$$c_{n,m}=[x^{m-n-N/2}+(1/x)^{m-n-N/2}]e^{iu(n+m)},$$

$$d_n=\frac{\cos u}{1/\rho+\cos u(x+1/x)}\,[x^{N/2-1}+(1/x)^{N/2-1}]e^{2iun}. \tag{A14}$$

Using this completely explicit form of the wave function, matrix elements can be calculated by straightforward summations of geometric progressions. For example, the norm $N_2=\langle\psi_2|\psi_2\rangle$ is found to be

$$N_2=\sum_{n=1}^{N-1}\sum_{m=n+1}^{N}|c_{n,m}|^2+\sum_{n=1}^{N}|d_n|^2$$
$$=\frac{Nx^2}{x^N}\left\{\frac{1}{1-x^2}+\left[\frac{\cos u}{1/\rho+\cos u(x+1/x)}\right]^2\right\}, \tag{A15}$$

where we have neglected in the bracket terms that vanish exponentially in the limit $N\to\infty$; e.g., $x^N\to 0$ because, generically, $0<x<1$.

The required matrix element $\langle\psi_2|\mu_x|\psi_1\rangle$ between the normalized one- and two-magnon states is now effected by noting that

$$\mu_x|\psi_1\rangle=\frac{1}{\sqrt{2N}}\left(\sum_{n=1}^{N-1}\sum_{m=n+1}^{N}c'_{n,m}|n,m\rangle+\sum_{n=1}^{N}d'_n|n,n\rangle\right)$$
$$+\sqrt{\frac{N}{2}}\,\delta(k)|\Omega\rangle,$$

$$c'_{n,m}=e^{ink}+e^{imk},\quad d'_n=e^{ikn}. \tag{A16}$$

Therefore

$$\langle\psi_2|\mu_x|\psi_1\rangle=\frac{1}{\sqrt{2NN_2}}\left(\sum_{n=1}^{N-1}\sum_{m=n+1}^{N}\overline{c_{n,m}}c'_{n,m}+\sum_{n=1}^{N}\overline{d_n}d'_n\right), \tag{A17}$$

where N_2 is the norm of Eq. (A15). A tedious but straightforward calculation of the sums shows that a nonvanishing matrix element is obtained only when the crystal momentum of the two-magnon state is equal (mod 2π) to the one-magnon momentum k, as expected. Hence we may write $\langle\psi_2|\mu_x|\psi_1\rangle\equiv f(k)$ whose explicit form for the single-ion bound state was already quoted in Eq. (3.22). One should recall that for this state $\cos u=-\cos(k/2)$, in accord with the zone folding discussed earlier.

The generalization of the preceding results to an antiferromagnetic chain is more or less straightforward. The fully ordered state is again an eigenstate of the Hamiltonian (4.1) and becomes the lowest-energy (ground) state for $h>h_c=1+4\rho$. Similarly the single-magnon state (A1) is an eigenstate with excitation energy given by Eq. (4.6). The excitation energy of the two-magnon bound states reads

$$E=2(h-h_c)+4\rho\left[1+\frac{1}{2}\left(x+\frac{1}{x}\right)\cos u\right], \tag{A18}$$

where x is any root of the cubic equation

$$\rho x^3-\frac{x^2}{\cos u}+(\rho+2)x-2\rho\,\cos u=0 \tag{A19}$$

in the interval [0,1]. The relevant roots are approximated near the zone boundary ($\cos u\sim 0$) by

$$x\approx\rho\,\cos u\quad\text{or}\quad 2\cos u \tag{A20}$$

and again correspond to a single-ion and an exchange bound state. A technical difference from the FM case is that both roots lie in [0,1] for $\cos u>0$. As a consequence, no folding of the zone is required for either mode and we may simply set $u=k/2$ in Eqs. (A18)–(A20) where k takes values in the fundamental zone.

The single-ion bound state is studied efficiently by the change of variables

$$x=\rho\,\cos\frac{k}{2}\,z;\quad z=1-\frac{\rho^3z^3\cos^2(k/2)}{2-\rho z}, \tag{A21}$$

where the cubic equation can be solved accurately by simple iteration starting with $z=1$. The result of a single iteration is sufficiently accurate for $\rho\ll 1$ and was stated in Eq. (4.8). Similarly the exchange bound state is sorted out by the change of variables

$$x=2\cos\frac{k}{2}\,w;\quad w=1-\frac{4\rho w^3\cos^2(k/2)}{\rho-2w}, \tag{A22}$$

and by iterating the cubic equation starting with $w=1$. The resulting spectrum was illustrated in Fig. 9 for a typical choice of parameters of current interest for which the single-ion dispersion is again well separated above the continuum. The main difference from the FM results of Fig. 4 is that the exchange bound state now branches off above the continuum. As a result, the bound-state spectrum is significantly different for large ρ. Thus the single-ion dispersion approaches but never touches the upper side of the continuum. Instead, the single-ion and exchange dispersions merge at the zone boundary for $\rho=2$ and exchange roles for $\rho>2$. For any finite ρ, however large, there is finite gap between the continuum and the bound state at the zone center; the gap behaves as $1/8\rho$ for large ρ and vanishes only in the extreme limit of vanishing anisotropy ($\rho\to\infty$) where the bound-state spectrum degenerates into a single dispersion that extends throughout the zone, just above the continuum. A related fact is that the matrix element quoted in Eq. (4.13) and plotted in Fig. 10 differs significantly from the FM results of Fig. 5, for it increases without bound at the zone center with increasing ρ. The picture described above for large ρ may prove to be useful for the study of antiferromagnetic chains in the Haldane phase ($\rho\gtrsim 1$) immersed in a sufficiently strong bias field ($h>1+4\rho$).

[1] I. Affleck, Phys. Rev. B **46**, 9002 (1992).
[2] H. Ohta, N. Makita, K. Yoshida, T. Nanba, and M. Motokawa, Int. J. Infrared Millim. Waves **13**, 457 (1992).
[3] H. Ohta and M. Motokawa, in *Recent Advances in Magnetism of Transition Metal Compounds*, edited by A. Kotani and N. Suzuki (World Scientific, Singapore, 1993), p. 316.
[4] S. A. Zvyagin, V. V. Eremenco, V. V. Pishko, A. Feher, M. Orendac, and A. Orendacova, Low Temp. Phys. **21**, 680 (1995).
[5] S. A. Zvyagin, T. Rieth, M. Sieling, S. Schmidt, and B. Lüthi, Czech. J. Phys. **46**, 1937 (1996).
[6] P. A. Lindgard, Physica B **120**, 190 (1983).
[7] N. Papanicolaou and P. Spathis, J. Phys.: Condens. Matter **1**, 5555 (1989); **2**, 6575 (1990); Phys. Rev. B **52**, 16 001 (1995).
[8] R. Siberglitt and J. B. Torrance, Jr., Phys. Rev. B **2**, 772 (1970).
[9] N. Papanicolaou and G. C. Psaltakis, Phys. Rev. B **35**, 342 (1987).
[10] N. Suzuki and J. Makino, J. Phys. Soc. Jpn. **64**, 2166 (1995).
[11] C. P. Slichter, *Principles of Magnetic Resonance* (Springer-Verlag, Berlin, 1978).
[12] T. Haseda, N. Wada, M. Hata, and K. Amaya, Physica B **108**, 841 (1981).
[13] M. Sieling (private communication).
[14] L. R. Mead and N. Papanicolaou, J. Math. Phys. (N.Y.) **25**, 2404 (1984).
[15] S. T. Chiu-Tsao, P. M. Levy, and C. Paulson , Phys. Rev. B **12**, 1819 (1975).
[16] R. P. Hodgson and J. B. Parkinson, J. Phys. C **18**, 6385 (1985).
[17] R. F. Wallis, D. L. Mills, and A. D. Boardman, Phys. Rev. B **52**, R3828 (1995).
[18] R. Lai, S. A. Kiselev, and A. J. Sievers, Phys. Rev. B **54**, R12 665 (1996).
[19] R. Orbach, Phys. Rev. **112**, 309 (1958).